Available online at www.CivileJournal.org

Civil Engineering Journal

(E-ISSN: 2476-3055; ISSN: 2676-6957)

Vol. 12, No. 05, May, 2026

Synthesis of Nano-Silicon Hybrid Alkyl Carboxylate to Inhibit Water and Chloride Transport in Concrete

Ruixing Chen [1, 2, 3*], Meng Yang [1], Zhen Liu [1], Yiming Ren [1], Pengyu Qian [1], Wenhua Zhang [1, 2, 3]

[1] *Department of Civil Engineering, Nanjing Forestry University, Nanjing 210037, China.*

[2] *Jiangsu Carbon Sequestration Materials and Structural Technology of Bamboo & Wood Research Center, Nanjing Forestry University, Nanjing 210037, China.*

[3] *Jiangsu Highway Intelligent Detection and Low-Carbon Maintenance Engineering Research Center, Nanjing Forestry University, Nanjing 210037, China.*

Received 23 February 2026; Revised 24 April 2026; Accepted 27 April 2026; Published 01 March 2026

Abstract

Concrete is vulnerable to water and chloride ingress because of its porous structure and hydrophilic hydration products. To address the poor dispersion, hydration interference, and strength loss often associated with conventional hydrophobic modifiers, this study synthesized a nano-silicon hybrid hydrophobic polymer ester (HPE) based on C12 alkyl carboxylate groups. Unlike conventional nano-silicon or alkyl-based modifiers that mainly rely on pore refinement or surface hydrophobization alone, HPE integrates C12 alkyl carboxylate groups with nano-silicon to construct multiple transport barriers. The effects of HPE dosage on concrete properties and transport-inhibition mechanisms were evaluated using contact angle, water absorption, electrical flux, rapid chloride migration, natural chloride diffusion, compressive strength, SEM, and MIP tests. HPE increased the contact angle from 14° to 78° and reduced long-term water absorption to 28% of the control. The electrical flux and chloride migration coefficient decreased to 48% and 62% of the control, respectively. MIP results showed reductions of 67.9% in the most probable pore diameter and 28.4% in total porosity. The enhanced durability is attributed to hydrophobic film formation, in-situ pore-blocking particles, and nano-silicon-assisted pore densification.

Keywords: Chloride Ions; Water Absorption; Concrete; Hydrophobic Polymer Ester; Pore Structure.

1. Introduction

Concrete structures exposed to marine and deicing-salt environments are continuously subjected to water and chloride ingress. Owing to the interconnected pore network and intrinsically hydrophilic surfaces of cement hydration products, moisture can be transported through capillary suction, pressure gradients, and concentration gradients, thereby carrying chloride ions into the concrete matrix and accelerating reinforcement corrosion, cracking, and durability deterioration [1, 2]. Reducing the transport of water and chloride ions is therefore a central objective in the durability design of concrete. Among various protection strategies, hydrophobic modification has attracted increasing attention because it can alter the wettability of cement-based materials and suppress liquid-phase transport without necessarily relying only on pore blocking or external densification [3-6].

Hydrophobic modification of cement-based materials is generally achieved through surface treatment or integral modification [3, 5, 7]. Surface treatments, such as silane/siloxane impregnation, fluoropolymer coatings, PDMS-based

* Corresponding author: crx31824@163.com

https://doi.org/10.28991/CEJ-2026-012-05-025

coatings, and organic–inorganic composite coatings, can form a low-surface-energy barrier on hardened concrete surfaces and substantially reduce water absorption and chloride penetration [8-12]. However, surface coatings are vulnerable to mechanical abrasion, ultraviolet aging, cracking, and insufficient penetration depth, which may limit their long-term effectiveness in harsh service environments [3, 8]. In contrast, integral hydrophobic modification introduces hydrophobic agents during mixing, enabling the modifier to distribute within the pore network and modify both internal pore walls and exposed surfaces. This approach can provide more persistent protection even when the external surface is partially damaged [5, 6, 13, 14]. Nevertheless, integral modification often faces challenges related to admixture dispersion, compatibility with cement hydration, workability loss, and strength reduction [10, 15-18].

The hydrophobic performance of organic modifiers is closely associated with the molecular structure of their hydrophobic groups, especially the length and mobility of alkyl chains. Alkyl groups with low surface energy can orient toward pore surfaces and reduce the affinity between water molecules and hydration products [5, 18-21]. Recent studies on alkyl-organosilane-modified cement pastes have shown that chain length strongly affects both hydrophobicity and hydration behavior. For example, methyl-, butyl-, octyl-, and dodecyl-trimethoxysilanes exhibit different effects on rheology, setting, hydration products, pore structure, and water resistance; intermediate or long alkyl chains generally enhance water repellency, whereas excessive chain length or dosage may impair workability or alter early-age reactions [5, 18, 22]. These findings indicate that molecular chain length is not merely a chemical parameter but a key factor controlling the balance between hydrophobic efficiency and cementitious compatibility.

Fatty-acid and carboxylate-based hydrophobic agents represent another important class of integral modifiers. In addition to hydrophobic modification, organic carboxylates, amines, azomethine polyester, and polyacrylamide-based compounds have also been reported to adsorb on steel or hydration-product surfaces, thereby improving resistance to chloride-induced corrosion in cementitious environments [23-26]. Stearic acid, calcium stearate, zinc stearate, oleic acid, and octadecane carboxylic acid have been used to reduce capillary water absorption and chloride ingress by forming hydrophobic films or insoluble metallic soaps within cement-based matrices. For instance, oleic-acid-modified fly ash has been incorporated into Portland cement to improve water resistance, while calcium stearate has been shown to reduce water absorption and chloride diffusion in concrete. [2, 27-30]. Octadecane carboxylic acid impregnation can also inhibit water and ion transport by modifying the wettability of C–S–H nanopores. Recent studies have also explored calcium-stearate-based hydrophobic concrete systems and synchronous integration between hydrophobic and ordinary concrete, further demonstrating the practical relevance of fatty-acid-salt modification strategies [29, 31]. However, these fatty-acid or carboxylate systems frequently show dosage-sensitive behavior. Although they improve hydrophobicity, excessive addition may introduce entrained air, weaken the interfacial transition zone, delay hydration, or increase porosity, ultimately reducing mechanical strength [27-29]. Therefore, the development of carboxylate-based hydrophobic agents requires a molecular design that simultaneously considers hydrophobic film formation, pore blocking, hydration compatibility, and strength retention.

However, single organic molecules or polymeric modifiers may suffer from poor dispersion, limited alkaline stability, or unstable interfacial behavior in cement pore solutions rich in hydroxyl and calcium ions [32-34]. To improve the dispersion and stability of hydrophobic modifiers, researchers have increasingly adopted carrier-based or organic–inorganic hybrid strategies. Industrial by-products and mineral particles, such as fly ash, silica fume, nano-SiO_2, and slag powder, can be surface-modified with hydrophobic molecules and then introduced into cementitious systems [2, 35-38]. Hydrophobic modification of fly ash provides a feasible route for converting hydrophilic supplementary cementitious materials into water-repellent fillers, whereas hydrophobic silica particles and silica fume can simultaneously contribute to pore refinement, microstructural densification, and surface hydrophobization [2, 36, 38]. Recent studies have further developed OTES@silica nanocapsules, nano-SiO_2-modified PDMS emulsions, PDMS@PMMA hydrophobic microcapsules, and engineered hydrophobic powders to improve water resistance while mitigating the adverse effects of pure organic hydrophobic agents on cement hydration [16, 21, 39, 40]. These studies suggest that nano-silica-assisted hybridization is a promising strategy because nano-SiO_2can improve particle dispersion, provide reactive silanol groups, participate in pozzolanic reactions, and compensate for the hydration-retarding or strength-reducing effects of organic hydrophobic components [21, 35, 40].

Despite these advances, several limitations remain. First, most existing studies have focused on silane/siloxane, PDMS, fluoropolymer, or fatty-acid salt systems, whereas alkyl carboxylate ester polymers with controllable chain structure have received comparatively limited attention in concrete durability applications [5, 10, 11, 15, 16, 18, 21, 27, 28]. Second, although the influence of alkyl chain length has been examined for organosilanes and fatty-acid derivatives, the role of C12 alkyl carboxylate ester structures in simultaneously regulating surface wettability, pore structure, and chloride transport remains insufficiently clarified [5, 18, 22]. Third, many hydrophobic systems rely on a single mechanism, such as surface film formation or pore blocking, while fewer studies have attempted to construct a multi-barrier system that integrates hydrophobic film formation, in situ precipitation, and nano-silica-assisted microstructural densification [21, 39, 40]. Consequently, there is still a need to develop an integral hydrophobic modifier that can achieve effective water/chloride transport inhibition while maintaining acceptable mechanical performance.

In this study, a nano-silicon hybrid alkyl carboxylate, denoted as hydrophobic polymer ester (HPE), was designed and synthesized using a C12-chain alkyl carboxylic ester precursor and a nano-silicon component. The design concept was based on the synergistic mechanism of surface hydrophobization, in situ pore blocking, and nano-silica-assisted

pore refinement. The C12 alkyl chain was selected to provide low-surface-energy hydrophobic groups, while the carboxylate/ester structure was expected to interact with calcium-containing hydration products and generate hydrophobic precipitates within capillary pores. Meanwhile, the nano-silicon component was introduced to enhance dispersion, interfacial compatibility, and microstructural densification. The effects of HPE dosage on surface wettability, capillary water absorption, electrical flux, rapid chloride migration, natural chloride diffusion, compressive strength, pore structure, and micro morphology were systematically investigated. Based on these results, the inhibition mechanism of HPE against water and chloride ion migration in concrete was elucidated, providing a molecular and microstructural basis for the design of integral hydrophobic modifiers for durable concrete.

2. Preparation and Structural Characterization of HPE

2.1. Design Concept of HPE

To address the common limitations of conventional hydrophobic modification materials for concrete, including poor dispersibility, interference with hydration, and insufficient long-term effectiveness, this study drew on previous experimental results and the findings of Wang et al. [20], which emphasize the critical role of long alkyl chains in constructing superhydrophobic surfaces. Accordingly, HPE was designed based on the synergistic mechanism of "pore filling-structural densification-surface hydrophobization".

At the molecular level, a C12 alkyl organic carboxylic acid was selected as the hydrophobic functional unit. The C12 chain was selected to balance hydrophobicity and cementitious compatibility. Previous studies showed that alkyl chain length affects hydrophobicity, hydration products, pore structure, and water absorption in cement pastes [3], while longer-chain C18 calcium stearate may improve water and chloride resistance but can cause pore coarsening and compressive strength loss [27]. Therefore, C12 was adopted as a medium-long chain to provide sufficient hydrophobicity while reducing the risk of poor dispersion and mechanical deterioration. Its carboxyl groups react with Ca^{2+} ions released from cement hydration products, generating insoluble hydrophobic particles in situ, thereby effectively blocking capillary pores. At the same time, this component self-assembles on the pore walls to form a continuous hydrophobic film, which markedly improves surface water repellency. To further enhance interfacial stability, a nano-silicon component was incorporated. This component facilitates the formation of a Si–O–C/Si–O–Si hybrid network, thereby improving the dispersion and compatibility of the modifier within the cement matrix.

A stepwise synthesis and controllable hybridization strategy was adopted for the preparation process. First, the carboxylate precursor was synthesized, it was then reacted with nano-silicon under catalytic and temperature-controlled conditions, and a stable aqueous dispersion system was finally obtained. This process effectively prevents nanoparticle agglomeration and ensures both the uniform dispersion of the modifier in concrete and its interaction with the cement matrix.

2.2. Preparation process of HPE

HPE was prepared through a two-step procedure, namely precursor synthesis followed by hybridization, as illustrated in Figure 1. First, the precursor was synthesized by uniformly mixing an organic solvent with a C12-chain organic carboxylic acid in a reactor under continuous stirring. The mixture was then gradually heated to 50–150 °C, after which polyether and a catalyst were then added. The reaction was allowed to proceed for 10–16 h to obtain a nano-precursor solution. Subsequently, the precursor underwent a hybridization reaction with nano-silicon under controlled temperature, pH, and stirring conditions. During this process, Si–O–C covalent bonds formed through condensation between the ester groups and silanol groups, generating an organic–inorganic hybrid structure. The final product was a stable nano-dispersion with a solid content of 18%, suitable for direct use as a hydrophobic treatment agent for concrete. Photographs of HPE and the nano-precursor solution are shown in Figure 2.

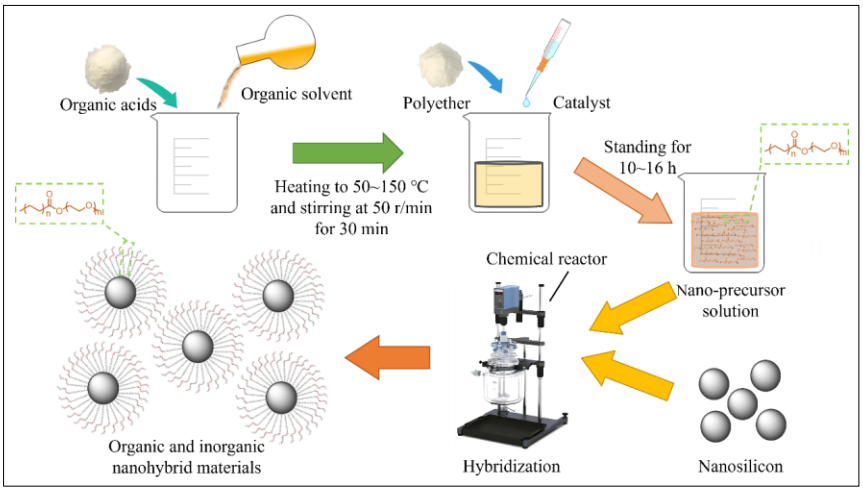

Figure 1. Preparation of HPE

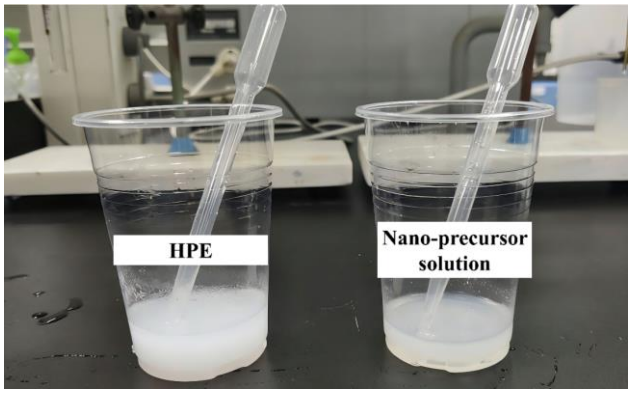

Figure 2. Appearance of HPE and the nano-precursor solution

2.3. Characterization of HPE

Scanning electron microscopy (SEM) images of the as-prepared HPE are presented in Figure 3. The chemical structure of HPE was characterized by Fourier-transform infrared spectroscopy (FT-IR), and the corresponding spectrum is shown in Figure 4. A distinct stretching vibration peak of the ester carbonyl group (C=O) was observed at approximately 1720 cm^{-1}, confirming the successful formation of the carboxylate structure. Characteristic peaks assigned to Si-O-C and Si–O–Si bonds appeared at approximately 1100 cm^{-1} and 800 cm^{-1}, respectively, indicating effective hybridization between the organic phase and the nano-silicon.

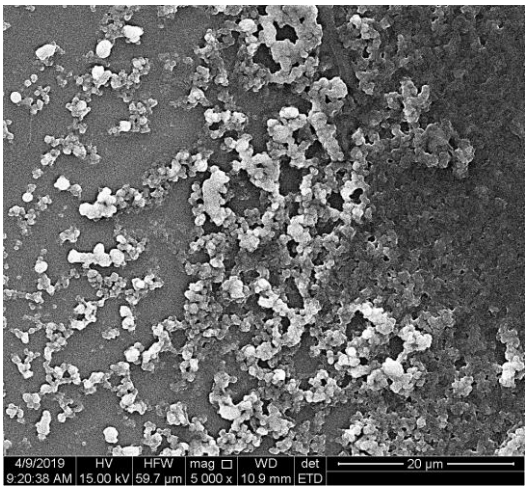

Figure 3. SEM images of HPE

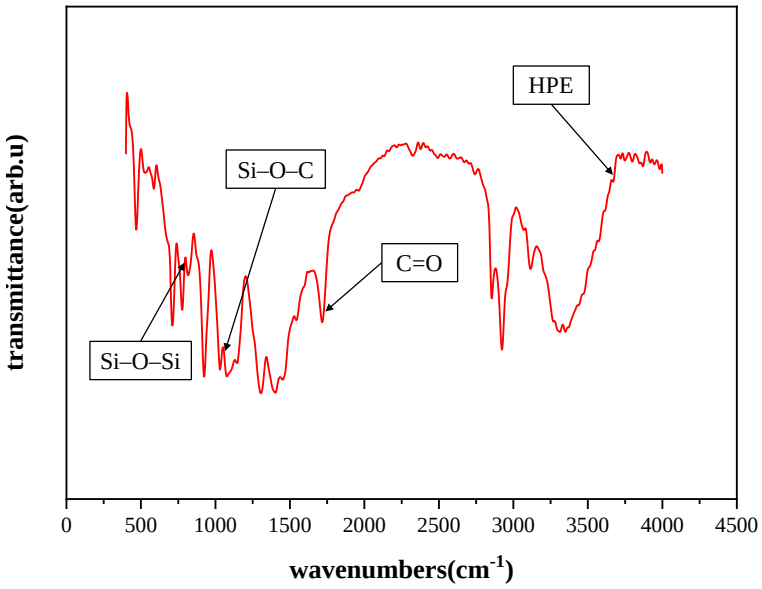

Figure 4. Fourier-transform infrared spectrum of HPE

3. Materials and Experimental Methods for Concrete

3.1. Materials

P.I 42.5 Portland cement was used, along with fly ash and slag as supplementary cementitious materials. River sand with a fineness modulus of 2.6 was used as the fine aggregate. Continuously graded crushed basalt (5-25 mm) with a water absorption of 1.3% was used as the coarse aggregate. Tap water was used for mixing. A polycarboxylate superplasticizer with a water-reduction rate of 28% was used to adjust workability. Analytical-grade sodium chloride and sodium hydroxide were used for the chloride ion migration and electrical flux tests. Ultrapure water, soluble starch, nitric acid, and silver nitrate were used for the titration of free chloride ions. The median particle sizes (D_{50}) of the cement, slag, and fly ash were 18.68, 9.12 and 20.35 μm, respectively, and their specific surface areas were 3231 cm²/g, 4120 cm²/g, and 3900 cm²/g, respectively. The particle size distributions are shown in Figure 5, and the chemical compositions are provided in Table 1.

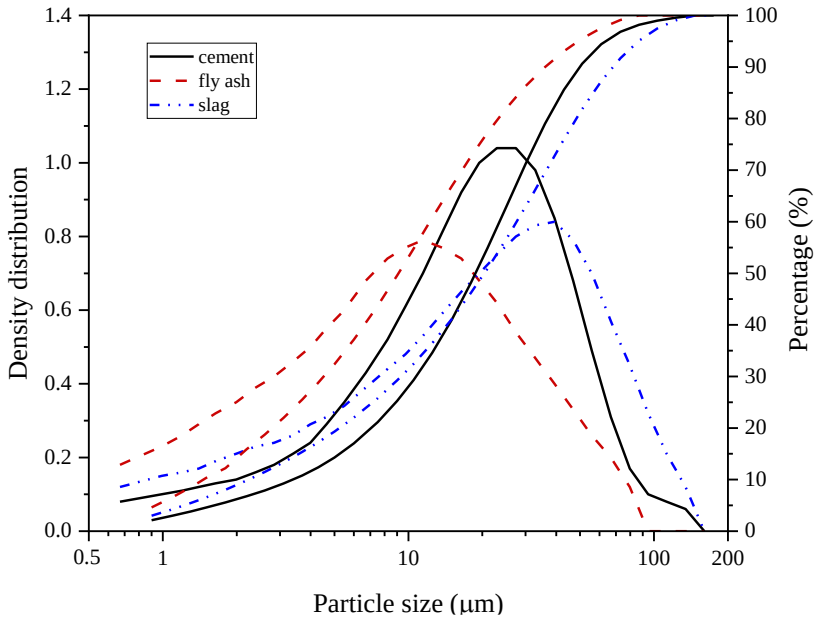

Figure 5. Particle size distribution and cumulative fractions of cement, fly ash, and slag

Table 1. Chemical compositions of cement, fly ash, and slag (%)

Oxide	CaO	SiO_2	Al_2O_3	Fe_2O_3	K_2O	MgO	Na_2O	SO_3	TiO_2
Cement	61.85	20.54	4.66	2.82	0.38	2.16	0.14	1.18	0.27
Fly ash	7.45	43.85	34.82	6.21	1.19	0.55	0.40	2.04	1.41
Slag	40.52	32.84	15.6	0.66	0.55	6.33	0.20	2.22	0.65

3.2. Specimen Preparation

The concrete mix proportions are listed in Table 2. The water-to-cement ratio was 0.4, the total cementitious material content was 490 kg/m³, the sand ratio was 41%, and the coarse-to-fine aggregate ratio was 6:4. To investigate the effect of HPE on the chloride ion penetration resistance of marine concrete, concrete specimens containing HPE dosages of 0%, 0.3%, 0.6%, 0.9%, 1.2%, and 1.8% were prepared. The dosage range of HPE was determined based on preliminary experimental experience, previous studies on carboxylic-acid-type hydrophobic admixtures, and practical considerations related to construction feasibility and material cost. Carboxylic-acid-type hydrophobic admixtures have been reported to significantly improve the water resistance and impermeability of cementitious materials within a moderate dosage range, although their effects on compressive strength, pore structure, and construction applicability should also be considered [41, 42]. Therefore, 1.8% was selected as the upper dosage limit to evaluate whether a higher HPE content could further enhance water and chloride transport resistance while avoiding excessive material cost and potential negative effects on concrete workability and mechanical performance. The solid content of HPE was 18%, and the water contained in HPE was included in the total mixing water. Corresponding cement paste specimens were also prepared for microstructural analysis.

Table 2. Mix proportions of concrete (kg/m^3)

Mark	Cement	Fly ash	Slag	Water	Sand	Fine aggregate	Coarse aggregate	HPE
HPE0	269.5	73.5	147.0	196.0	702.7	404.5	606.8	0.00
HPE0.3	269.5	73.5	147.0	189.3	702.7	404.5	606.8	8.17
HPE0.6	269.5	73.5	147.0	182.6	702.7	404.5	606.8	16.33
HPE0.9	269.5	73.5	147.0	175.9	702.7	404.5	606.8	24.50
HPE1.2	269.5	73.5	147.0	169.2	702.7	404.5	606.8	32.70
HPE1.8	269.5	73.5	147.0	155.8	702.7	404.5	606.8	49.00

The concrete specimen preparation procedure is illustrated in Figure 6. First, the cementitious materials and aggregates were dry-mixed for 3 min; then, water and the HPE solution were added and mixed for 1 min; finally, the water reducer was added and mixed for an additional 1 min. The concrete specimens were cured under standard curing conditions (20 ± 2 °C, RH ≥ 95%) before subsequent performance testing.

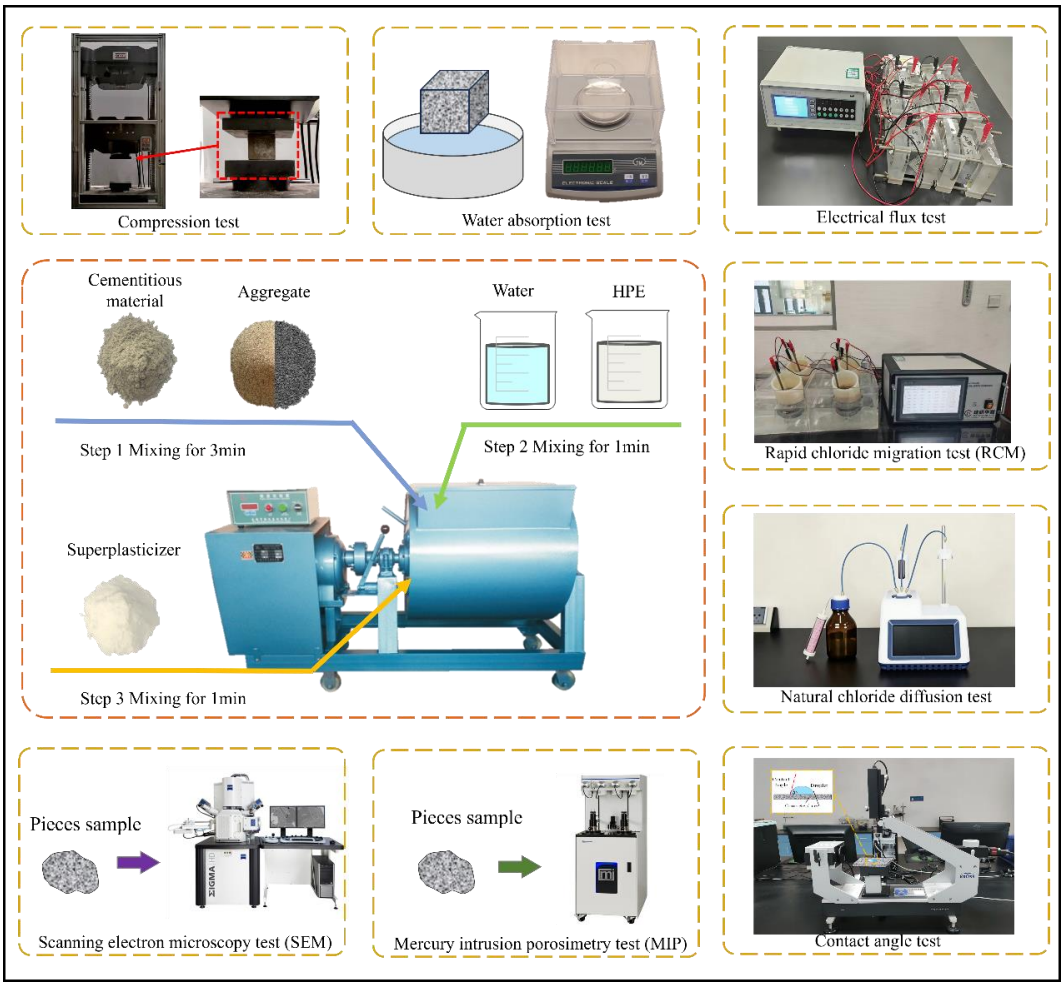

Figure 6. Preparation and testing procedure for HPE-modified concrete

3.3. Experimental Methods

3.3.1. Compressive Strength Test

The compressive strength of concrete was measured at 28 days in accordance with Chinese Standard GB/T 50081-2002. Three specimens were tested for each group, and the average value was reported as the test result.

3.3.2. Water Absorption Test

The water absorption test was conducted in accordance with BS 1881-122:2011. To prevent ettringite decomposition and structural damage caused by high temperature, the drying condition was modified to 100 °C for 72 h. This modified drying condition was adopted to reduce possible thermal damage to hydration products and pore structure, because excessive drying temperature may alter the moisture state and capillary absorption behavior of cementitious materials [43, 44]. In addition, severe high-temperature vaporization is not fully consistent with practical engineering exposure

conditions. Since all specimens were subjected to the same drying procedure, the comparison among different HPE dosages remains valid; however, comparisons with other studies should consider differences in drying and preconditioning methods. After cooling, the initial mass (m_0) was recorded. The specimens were then immersed in water to a depth of 20 mm in water and weighed at specified intervals to obtain m_t, where the subscript t denotes the water absorption time. The water absorption rate φ was calculated using the following equation:

$$\varphi=\frac{m_t-m_0}{m_0}\times 100\% \quad (1)$$

3.3.3. Electrical Flux Test

The resistance to chloride penetration was evaluated using the electrical flux method in accordance with GB/T 50082-2009. Concrete specimens were prepared as cylinders with a diameter of 100 mm and a height of 50 mm. After side sealing and vacuum saturation, the specimens were mounted in the test cell, with the cathode chamber filled with 3.0% NaCl solution and the anode chamber filled with 0.3 mol/L NaOH solution. Current values were recorded during the test, and the total electrical flux was calculated using the following equation:

$$Q=900(I_0+2I_{30}+2I_{60}+\ldots+2I_{300}+2I_{330}+I_{360}) \quad (2)$$

where, Q is the total electrical flux passing through the specimen (C), and It is the current at time t (A), recorded to an accuracy of 0.001 A

3.3.4. Rapid Chloride Migration Test (RCM)

The specimen preparation procedure was the same as that used for the electrical flux test, except that the vacuum saturation solution was replaced with saturated $Ca(OH)_2$ solution. Each specimen, sealed in a rubber sleeve and filled with 0.3 mol/L NaOH, was immersed in a cathode tank containing 10% NaCl solution. The selected voltage was applied in accordance with the relevant standard, and the initial and final temperatures of the solution were recorded. After the test, the specimens were split to expose the cross-sections, which were then sprayed with 0.1 mol/L $AgNO_3$ solution. After 15 min, the distance from the chromogenic boundary line to the bottom surface was measured, with at least five valid measurement points required. The non-steady-state chloride diffusion coefficient was calculated using Equation 3:

$$D_{nssm}=\frac{0.0239(273+T)}{(U-2)t}\left\{x_d-0.0238\sqrt{\frac{(273+T)Lx_d}{U-2}}\right\} \quad (3)$$

where, D_{nssm} is the non-steady-state chloride migration coefficient ($\times 10^{-12}$ m²/s), U is the applied voltage (V), T is the average temperature of the anolyte (℃), L is the specimen thickness (mm), t is the test duration (h), and X_d is the average chloride penetration depth measured by silver nitrate colorimetry (mm).

3.3.5. Natural Chloride Diffusion Test

The chloride ion penetration test was conducted in accordance with NT Build 443. After curing, all surfaces of the specimens except the exposed face were sealed with resin. The specimens were water-saturated and then immersed in a 165 g/L NaCl solution in a closed container, with an exposed area-to-solution volume ratio of approximately 25 cm²/L. The solution was replaced every five weeks, and the container was shaken weekly. After immersion, powder samples were collected by grinding inward from the exposed surface at 1-2 mm intervals. The acid-soluble chloride content was determined according to JGJ/T 322-2013, whereas free chloride ions were measured by silver nitrate titration.

Chloride concentration profiles were fitted by the least-squares method using the error-function solution of Fick's second law to determine the surface chloride concentration (Cs) and the non-steady-state diffusion coefficient (D_{nss}). The first data point near the surface was generally excluded during fitting. The fitting equation is given as follows:

$$C_x=C_i+(C_s-C_i\left\{1-erf\left[\frac{x}{2\sqrt{D_{nss}\cdot t}}\right]\right\} \quad (4)$$

where, C_x is the chloride ion concentration at depth x and exposure time t (%), C_i is the initial chloride ion concentration in the concrete (%), x is the distance from the mid-depth of the ground layer to the exposed surface (m), and t is the immersion time (s).

3.3.6. Contact Angle Test

The contact angle was measured to characterize the surface wettability of the materials. Cement paste specimens were sliced, dried at 40 °C for 48 h, and then conditioned in a constant-temperature and constant-humidity environment for 24 h. The tests were performed using a Drop Shape Analyzer DSA25; the test setup and droplet morphology are shown in Figure 7. Each specimen was placed on the stage, and a water droplet was dispensed onto its surface. The process was recorded using a high-speed camera, and the contact angle was analyzed with the accompanying software.

Three parallel measurements were conducted for each group. Because cementitious materials are absorbent, contact angles were recorded at 1 s and 30 s after the droplet contacted the surface

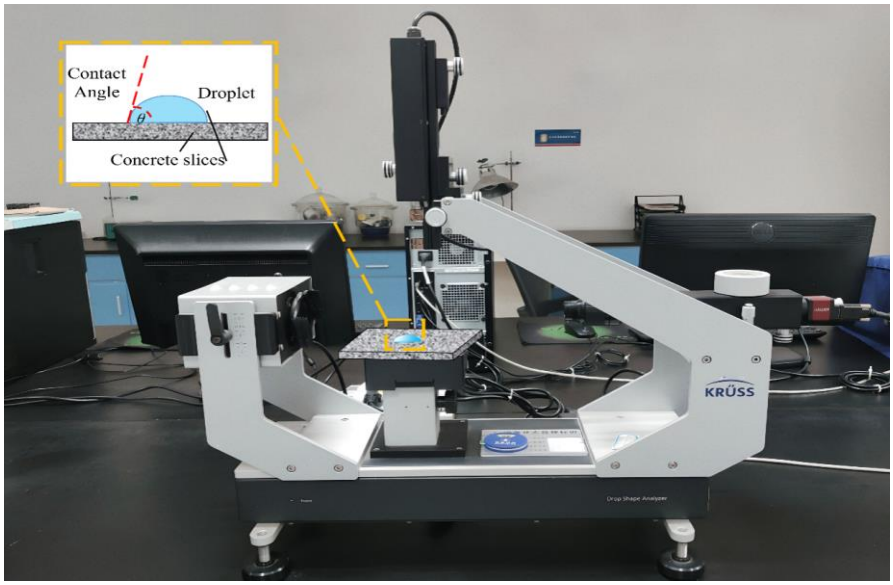

Figure 7. Contact angle instrument and representative droplet image

3.3.7. Mercury Intrusion Porosimetry Test (MIP)

The pore structure of cement-based materials was characterized by mercury intrusion porosimetry (MIP). Cement paste specimens at the specified ages were crushed into 3-8 mm particles, and hydration was stopped using anhydrous ethanol, which was replaced after 12 h and maintained for 48 h. After vacuum drying at 40 °C for 48 h, the test was conducted using an AutoPore IV 9510 mercury porosimeter. The mercury surface tension and contact angle were set to 480 mN/m and 140°, respectively. The pressure ranges were 1.5-350 kPa for the low-pressure stage and 140-420 MPa for the high-pressure stage, both under scanning mode.

3.3.8. Scanning Electron Microscopy Test (SEM)

The micromorphology of cement pastes was observed using a field-emission scanning electron microscope (FEI Quanta 250). The samples were crushed and soaked in isopropanol for 24 h, followed by vacuum drying at 35 °C for 72 h. Before testing, the samples were fractured to obtain fresh cross-sections and then sputter-coated with gold to avoid charge accumulation.

4. Results and Discussion

4.1. Surface Hydrophobicity and Contact Angle Evolution

As shown in Figure 8, the effect of HPE on the surface water behavior of cement paste is directly reflected in the droplet spreading and penetration morphology. In the reference group (Figure 8-a), the droplet contact edge spread rapidly and was quickly absorbed, whereas in the HPE-modified groups (Figure 8-b), the droplet edge showed almost no spreading and the water penetration rate decreased markedly. This phenomenon indicates that HPE altered the water transport mechanism from rapid capillary absorption to a slower process dominated by the hydrophobic interface, thereby substantially improving the resistance of cement paste to instantaneous water erosion. Among all samples, the specimen containing 1.8% HPE exhibited the most pronounced effect.

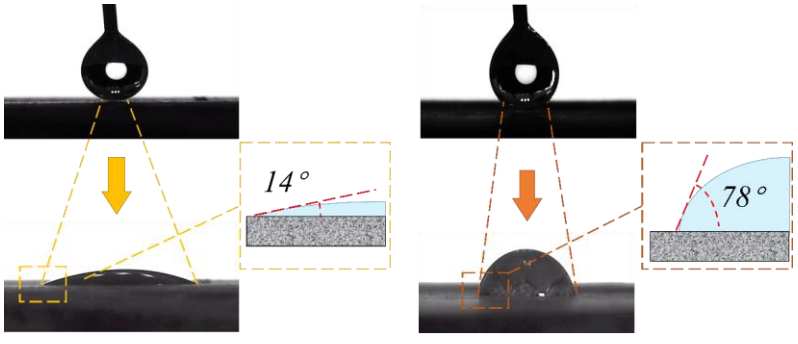

(a) (b)

Figure 8. Significant increase in contact angle: water droplet behavior on (a) reference and (b) HPE-modified cement paste surfaces

The contact angle test results for samples with different HPE dosages (Figure 9) further support the above observations. At 1 s after droplet contact, the contact angle of the reference group (HPE0) was only 14°, whereas that of the sample containing 1.8% HPE increased to 78°. When the contact time was extended to 30 s, the contact angles of all samples decreased to some extent because of the inherent water absorption of cement-based materials; however, the sample containing 1.8% HPE still maintained a contact angle of 54°, which was substantially higher than that of the reference group. These results indicate that HPE can markedly increase the contact angle of the cement matrix surface, and that this effect becomes stronger as the HPE dosage increases.

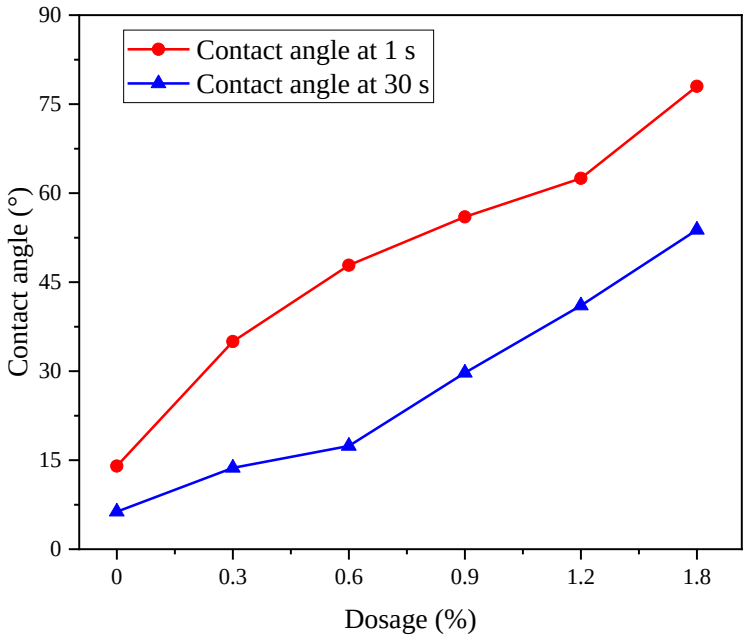

Figure 9. Contact angles of cement pastes with different HPE dosages measured at 1 s and 30 s

Compared with previously reported superhydrophobic cement-based materials, the contact angle obtained in this study was moderate but mechanically more balanced. Luo et al. [45] reported that increasing the dosage of isobutyltriethoxysilane progressively increased the contact angle of cement-based materials, reaching 158.3°, but this was accompanied by a significant reduction in compressive strength. They further showed that a composite hydrophobic-agent system could maintain a similar contact angle while achieving a 68% higher compressive strength than the corresponding single-agent system [45].

In the present study, the maximum contact angle of HPE-modified cement paste was 78° at 1s and remained 54° after 30s. Although HPE did not produce a superhydrophobic surface, it substantially altered the wetting behavior and reduced long-term water absorption to 28% of that of the reference concrete, while maintaining relatively limited strength loss. This indicates that the performance advantage of HPE lies in balancing hydrophobicity, transport resistance, and mechanical integrity rather than maximizing contact angle alone.

4.2. Effect of HPE-induced Hydrophobicity on Capillary Water Uptake in Concrete

As a hydrophilic porous material, concrete contains a multiscale pore structure that tends to induce strong capillary action. An increase in the contact angle of concrete directly reduces the driving force for capillary water absorption. According to the capillary rise equation shown in Equation 5, an increase in the contact angle θ decreases the value of cos θ, thereby markedly reducing the capillary rise height h. This effect becomes more pronounced as the pore radius r decreases (Figure 10-a).

$$h = \frac{2\sigma cos\theta}{\rho g r} \quad (5)$$

where, h is the capillary rise height (m), r is the capillary pore radius (m), σ is the surface tension of water (N/m), θ is the contact angle (°), ρ is the density of water (kg/m³), and g is the gravitational acceleration (m/s²).

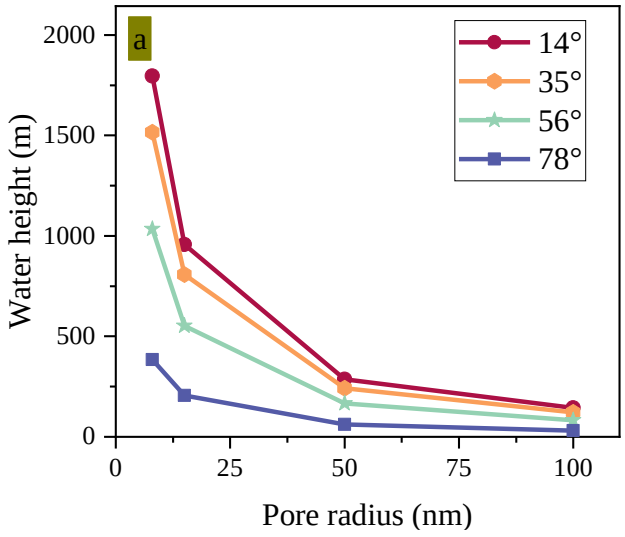

(a) Capillary rise height

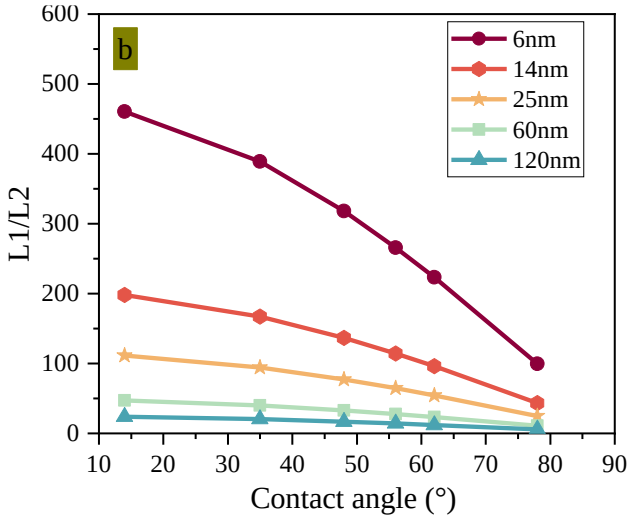

(b) Pore-filling resistance (L_1 /L_2)

Figure 10. Effects of contact angle on capillary transport properties

To quantitatively analyze the influence of the contact angle on the water-filling process in capillary pores, a physical model based on gas compression equilibrium was employed [27]. This model assumes cylindrical capillary pores. Initially, an air column with a length of L_1 is compressed to a length of L_2 after water ingress, with no gas escaping. According to this model, the ratio L_1/L_2, which reflects the water-filling state of the pore, is expressed by Equation 6.

$$\frac{L_1}{L_2} = \frac{2\sigma cos\theta}{rP} + 1 \quad (6)$$

where, P is the air pressure (Pa).

Figure 10-b shows the effect of the contact angle on L_1/L_2 for different pore radii. Taking capillary pores with a radius of 8 nm as an example, the L_1/L_2 value of the reference cement paste was 174 , whereas that of the sample containing 1.8% HPE decreased to 37. This decrease indicates that HPE limits water filling in nanoscale capillary pores by enhancing interfacial hydrophobicity.

Figure 11 presents the time-dependent water absorption of concrete with different HPE dosages. The water absorption process of the control concrete follows a typical two-stage pattern, with rapid initial uptake during the first 7 h followed by a slower stage. By contrast, after HPE incorporation, the time-dependent water absorption curves no longer exhibit an obvious two-stage behavior, and the water absorption decreases markedly with increasing HPE dosage. After 540 h, the water absorption of concrete containing 1.8% HPE was only approximately 28% of that of the control group.

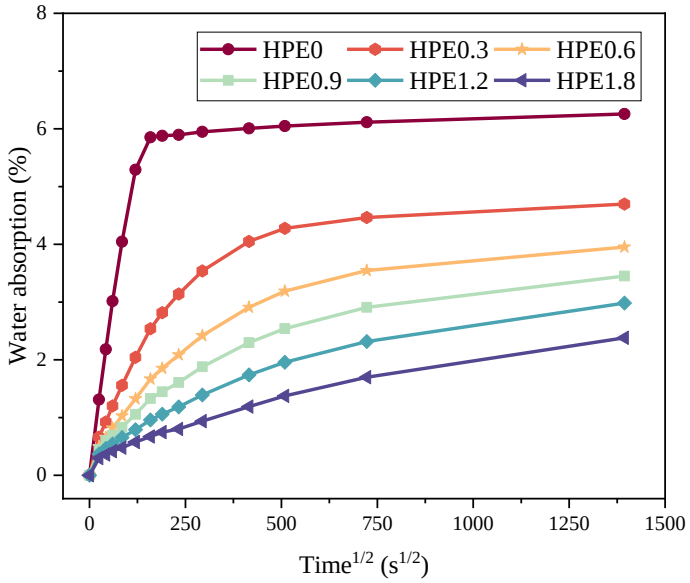

Figure 11. Effect of HPE on water absorption in concrete

The water absorption rate was quantified using Equation 7. Figure 12 illustrates the effect of HPE on the water absorption rate of concrete. The water absorption rate of concrete decreases markedly with increasing water absorption time; meanwhile, it also declines as the HPE dosage increases, with HPE exerting a more pronounced effect on the early-stage water absorption rate. As shown in the magnified view of Figure 12, HPE continued to reduce the water absorption rate even after a prolonged period of 22.5 days (540 h). This result confirms the long-term stability of the hydrophobic barrier provided by HPE.

$$P_W = \frac{\varphi}{A \cdot t} \tag{7}$$

where, *Pw* is the water absorption rate of concrete (m^{-2} s^{-1}), φ is the water absorption of concrete (%), A is the surface area (m^2), and t is the time (s).

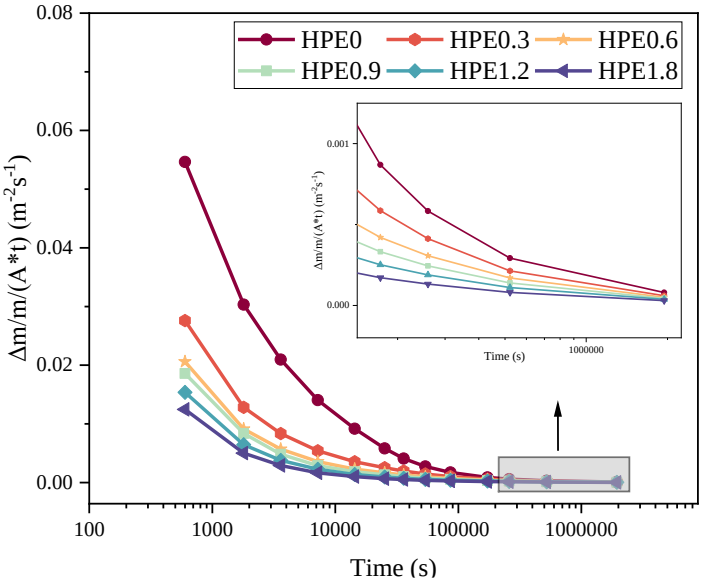

Figure 12. Water absorption rate of concretes as a function of time

4.3. Chloride in Penetration Resistance of Concrete

Figure 13 presents the 28-day electrical flux and chloride ion migration coefficient (RCM) of concrete with different HPE dosages. The results show that HPE significantly reduces both parameters. As the HPE dosage increases, the electrical flux and chloride ion migration coefficient first decrease rapidly and then tend to stabilize within the dosage range of 0.3%-0.9%, followed by a further decrease at higher dosages. At a dosage of 1.8%, the electrical flux of concrete reached its minimum value, corresponding to 48% of that of the control group, whereas the chloride ion migration coefficient reached its minimum at a dosage of 1.2%, corresponding to 62% of that of the control group. These findings indicate that HPE effectively impedes ion migration in concrete under an applied electric field.

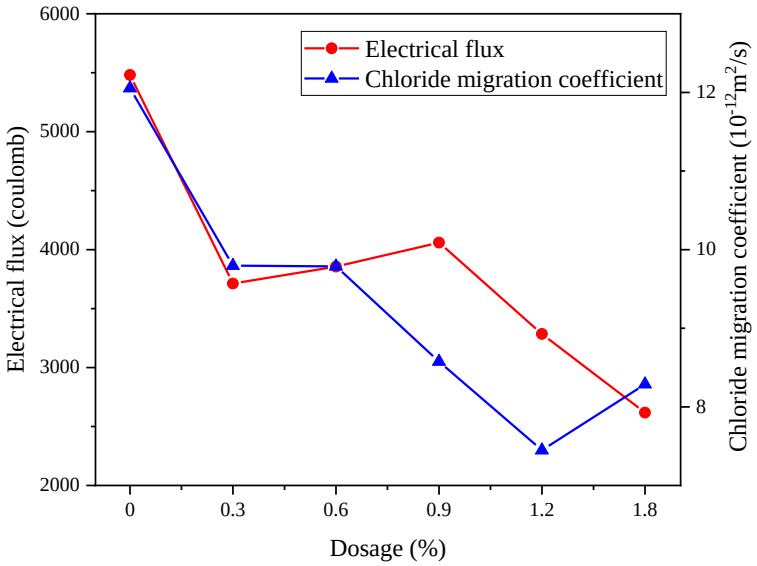

Figure 13. Ratios of electrical flux and chloride diffusion coefficient of concrete with different HPE dosages

This result is comparable to recent bulk hydrophobic powder modification systems designed to hinder water-salt transport. Yu et al. reported that PDMS-modified hydrophobic cement powder reduced water absorption and chloride diffusion coefficient by up to 40% and 82%, respectively, while maintaining a relatively limited 28-day strength reduction of approximately 10% [46]. In the present study, HPE reduced the electrical flux and RCM chloride migration coefficient to 48% and 62% of those of the control group, respectively. Although the reduction in chloride migration coefficient was lower than that reported for the hydrophobic cement powder system, HPE achieved simultaneous reductions in electrical flux, chloride migration, natural chloride content, and pore size. This suggests that HPE inhibits chloride transport through a combined mechanism involving hydrophobic film formation, in situ pore blocking, and nano-silicon-assisted pore refinement.

Figure 14 presents the chloride ion contents and fitting curves of concrete with different HPE dosages after immersion in sodium chloride solution for 57 days. The results show that HPE incorporation significantly reduces the acid-soluble chloride ion content at different depths in concrete. When the dosage was below 1.2%, the chloride ion content in concrete continuously decreased with increasing HPE dosage; however, when the dosage increased from 1.2% to 1.8%, no further significant reduction was observed. Notably, in the shallow layer (penetration depth < 5 mm), concrete containing 1.2% HPE exhibited the lowest acid-soluble chloride ion content, whereas in the deeper layer (> 5 mm), concrete containing 1.8% HPE showed the best chloride penetration resistance.

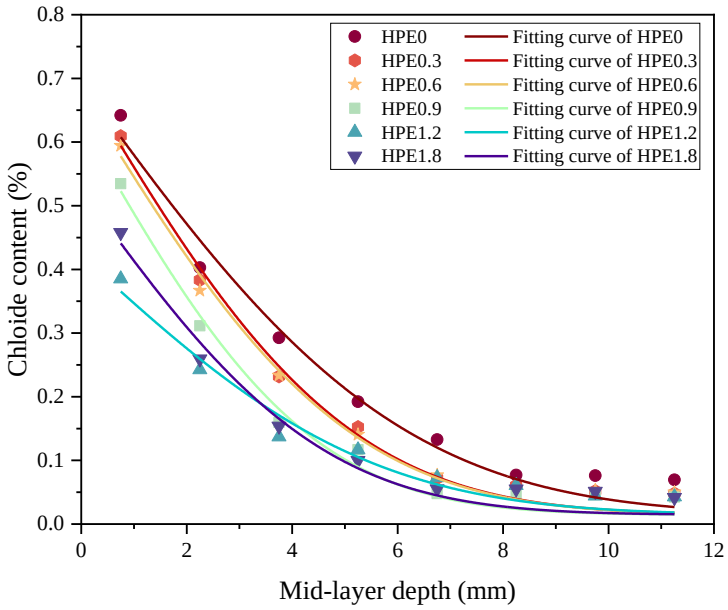

Figure 14. Acid-soluble chloride content in concrete with different HPE dosages

Figure 15 shows the effect of HPE on the free chloride ion content in concrete. Similar to the trend observed for acid-soluble chloride ions, HPE effectively reduced the free chloride ion content in concrete. When the dosage did not exceed 1.2%, the reduction effect became more pronounced as the dosage increased. A comparison of Figure 14 and 15 shows that HPE incorporation not only reduces the total chloride ingress in concrete, represented by acid-soluble chloride ions, but also markedly decreases the concentration of free chloride ions with corrosive activity. This suggests that the hydrophobic environment and reaction products formed by HPE may enhance chloride binding, converting more free chloride ions into bound chloride ions and thereby further weakening their corrosive potential.

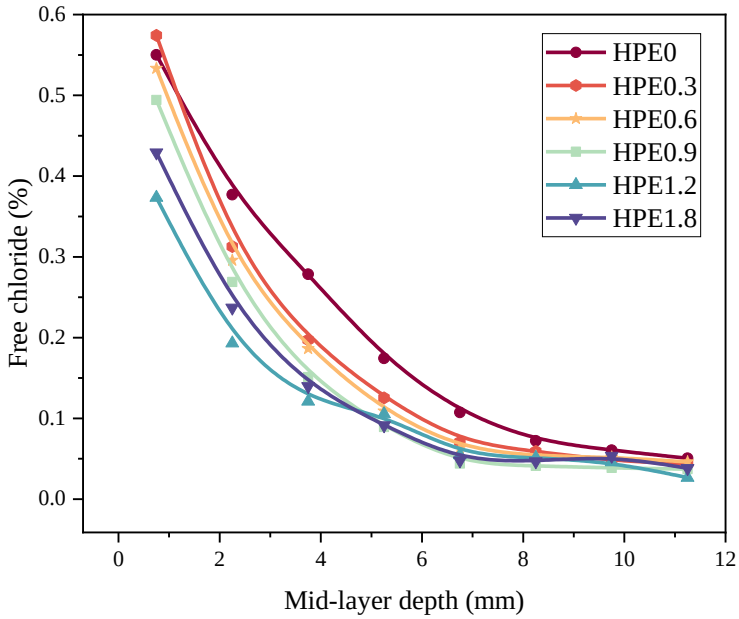

Figure 15. Free chloride content in concrete with different HPE dosages

Based on Equation 4 and the chloride ion concentration distribution profiles, the chloride ion migration coefficient D_{nss} and surface chloride concentration C_s of concrete were obtained by fitting, and the results are listed in Table 3. Overall, HPE effectively reduced the chloride ion migration coefficient of concrete. With increasing HPE dosage, D□□□ in concrete exhibits a trend of first decreased and then increased, reaching a minimum at a dosage of 0.9%; by contrast, Cs first increased and then decreased, with the lowest value observed at a dosage of 1.2%.

Table 3. Chloride diffusion coefficient (D_{nss}) and surface chloride content (C_s) calculated using the standard method

Parameter	HPE0	HPE0.3	HPE0.6	HPE0.9	HPE1.2	HPE1.8
D_{nss}	3.09	1.92	1.97	1.55	2.85	2.06
C_s	0.57	0.61	0.58	0.52	0.33	0.39
R^2	0.98	0.98	0.98	0.98	0.98	0.95

It should be noted that the standard fitting results show that the surface chloride ion concentrations C_s of concrete containing 1.2% and 1.8% HPE were even lower than the measured values at a depth of 0.75 mm. This result is inconsistent with the physical mechanism of chloride diffusion from the surface to the interior of concrete, indicating that the standard fitting method may be invalid under these conditions. Therefore, this study adopted a fixed surface chloride concentration method, in which the average *Cs* value of the groups with HPE dosages of 0%-0.6% was used as the boundary condition, and univariate constrained optimization was performed to recalculate D_{nss}. The results are shown in Figure 16. After this treatment, D_{nss} exhibited a more reasonable monotonic decreasing trend with increasing HPE dosage, reaching its minimum at a dosage of 1.2%. This result is consistent with the trends observed for macroscopic properties such as water absorption rate and electrical flux, confirming that HPE can continuously and effectively retard chloride ion diffusion in concrete.

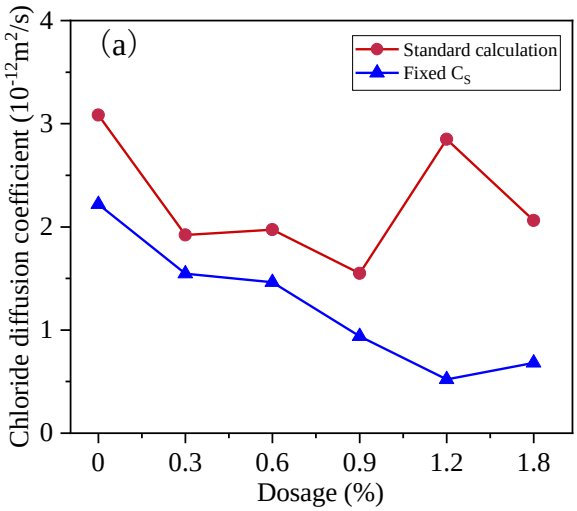

(a) Standard fitting method

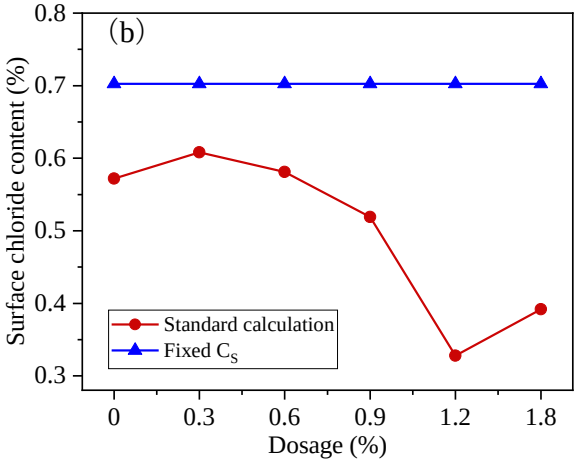

(b) Constrained method with fixed surface concentration

Figure 16. Comparison of methods for determining chloride diffusivity

4.4. Compressive Strength of Concrete

Figure 17 presents the effect of HPE on the 28-day compressive strength of concrete. As the HPE dosage increased, the compressive strength first decreased and then rebounded slightly. At HPE dosages of 0.3%, 0.6%, 0.9%, 1.2%, and 1.8%, the compressive strength decreased by approximately 7.2%, 5.2%, 17.7%, 13.3%, and 6.1%, respectively. Notably, common hydrophobic admixtures reported in the literature may cause compressive strength reductions of more than 30% in concrete [28, 47, 48], whereas the strength loss caused by HPE in this study was relatively limited.

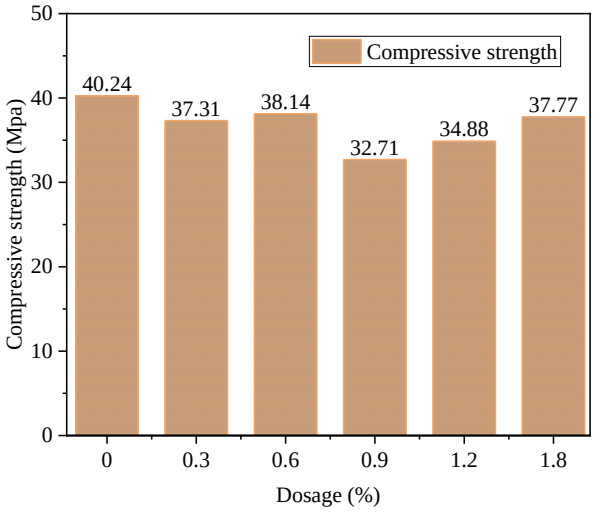

Figure 17. Effect of HPE on the 28-day compressive strength of concrete

A comparison with recent hydrophobic powder systems further highlights the strength-retention advantage of HPE. Zhao et al. prepared an engineered hydrophobic slag powder and reported that the 28-day compressive strength of the modified paste increased by 22.6%, which was attributed to the synergistic effects of slag reactivity, particle filling, and controlled hydrophobic modification [49]. Yu et al. developed a PDMS-modified hydrophobic cement powder and found that, although water absorption and chloride diffusion were markedly reduced, the 28-day strength still decreased slightly by approximately 10% [46]. In the present study, HPE caused a maximum strength reduction of 17.7% at 0.9%, but the strength recovered at higher dosages, with only a 6.1% reduction at 1.8%. This recovery indicates that the nano-silicon hybrid structure partly compensated for the weakening effect of the organic hydrophobic groups through pore refinement and matrix densification.

From a mechanistic perspective, each 1% increase in the porosity of cement-based materials can lead to a 4%-6% reduction in compressive strength. Although HPE effectively reduced the porosity of cement paste, this effect did not fully offset its negative influence on strength. This behavior can be primarily attributed to two factors. First, the hydrophobic groups in HPE become embedded in the cement hydration products, weakening the bonding strength of the hardened cement paste. Second, HPE changes the surface properties of the cement paste by increasing the contact angle, which causes water in the paste to accumulate toward the interfacial transition zone of the concrete. This, in turn, reduces the bonding strength among the interfacial transition zone, aggregates, and cement paste after hydration. Together, these effects contribute to the decrease in concrete strength, which is consistent with the findings of Yu et al. [50].

4.5. Microstructure: Pore Structure and Hydration Products

Mercury intrusion porosimetry (MIP) results revealed that HPE significantly optimized the pore structure of hardened cement paste. The cumulative mercury intrusion curves and differential pore size distribution curves are shown in Figures 18-a and 18-b, respectively. The key pore structure parameters of concrete are listed in Table 4. The data show that HPE incorporation continuously improved the pore characteristics of the paste: the most probable pore size decreased substantially from 56.53 nm in the reference group to 18.17 nm in the group containing 1.8% HPE, corresponding to a reduction of 67.9%; the total porosity decreased from 22.88% to 16.39%, representing a reduction of 6.49 percentage points; and the median and average pore sizes showed similar decreasing trends. These results collectively confirm that HPE not only reduces the total porosity of the cement paste but, more importantly, refines and densifies the pore size distribution.

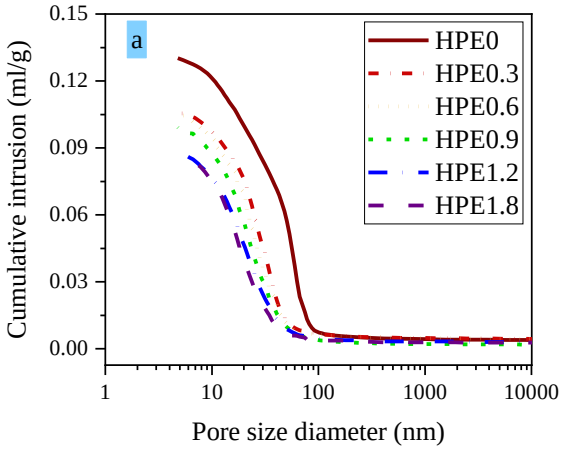

(a) Cumulative mercury intrusion pore volume

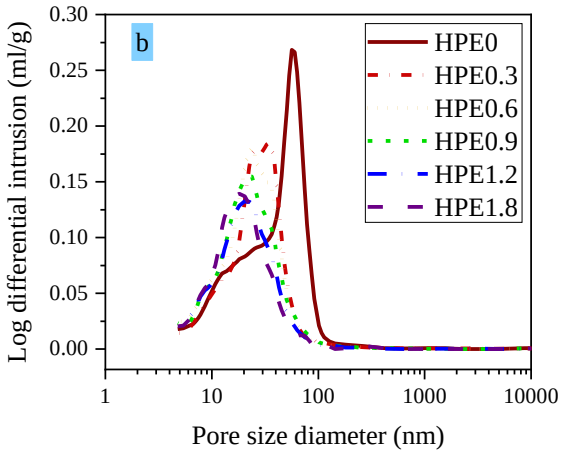

(b) Pore size distribution

Figure 18. Pore structure characteristics of HPE-modified cement paste

Table 4. Median pore diameter, average pore diameter, most probable pore diameter, and total porosity determined by MIP

Sample mark	Median pore diameter (volume) (nm)	Average pore diameter (4V/A) (nm)	Most probable pore diameter (nm)	Porosity (%)
HPE0	45.41	26.86	56.53	22.88
HPE0.3	27.22	21.70	34.62	19.14
HPE0.6	28.51	23.75	23.78	21.99
HPE0.9	22.07	18.25	22.54	18.31
HPE1.2	20.96	17.36	20.40	16.57
HPE1.8	18.72	16.44	18.17	16.39

The optimized pore structure provides a microstructural explanation for the reduced chloride transport. Previous studies have shown that chloride diffusion in cement-based materials is closely related to pore structure parameters, especially capillary porosity, total pore volume, and pore connectivity [51, 52]. In this study, HPE reduced the total porosity from 22.88% to 16.39% and decreased the most probable pore diameter from 56.53 nm to 18.17 nm. This refinement reduced the volume and continuity of connected capillary pores, thereby increasing the tortuosity of chloride transport paths and contributing to the reductions in electrical flux, chloride migration coefficient, and chloride content.

The SEM images in Figure 19 show the micromorphology of the reference group (a-c) and the group containing 1.2% HPE (d-f). Typical hydration products, including acicular ettringite, massive calcium hydroxide (CH), and layered C-S-H gel, are observed in both groups. Compared with the reference group, the HPE-modified samples show two distinct features. First, precipitated particles generated by the reaction between HPE and cement hydration products, such as CH, are visible on the C-S-H gel clusters (Figure 19-e). Second, a formed hydrophobic film can be observed on the inner walls of pores in the cement paste (Figure 19-f). These in situ generated hydrophobic particles can effectively block capillary pores, whereas the hydrophobic film on the pore walls fundamentally alters the wettability of the pore surface. Their synergistic effect provides direct microscopic evidence for the reduction in porosity and the enhancement of hydrophobicity.

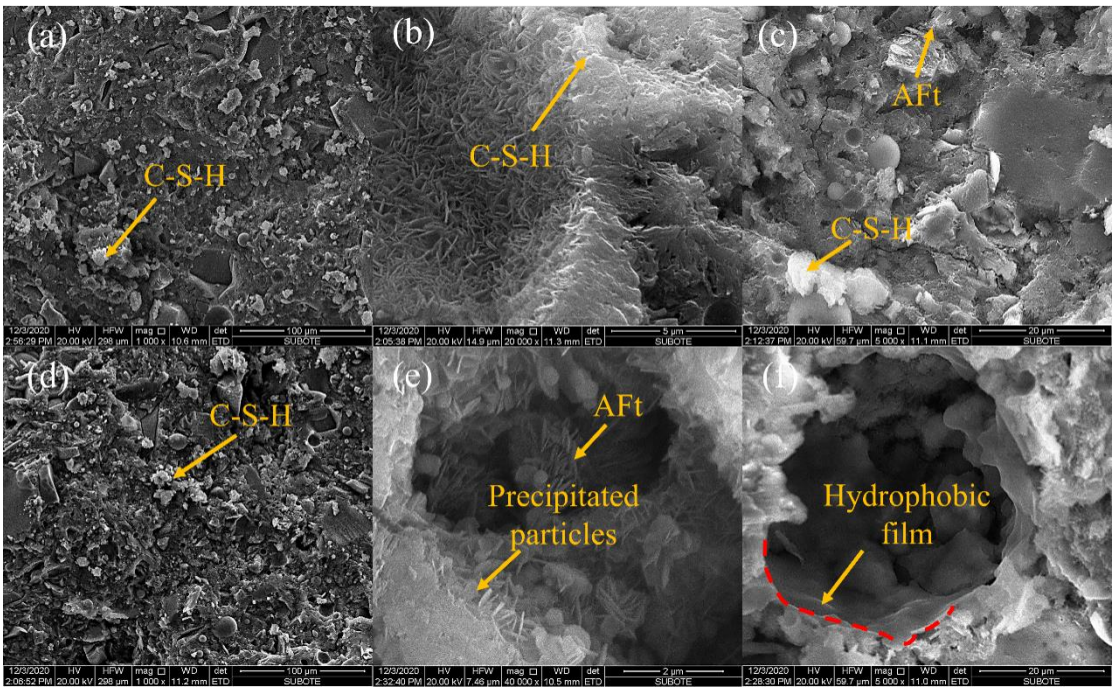

Figure 19. SEM images of cement pastes observed at 28 days. The upper images (a-c) were obtained from the reference sample, and the lower images (d-f) were obtained from the HPE-modified sample

4.6. Comprehensive Analysis of the Transport Inhibition Mechanism

Figure 20 schematically illustrates the mechanism by which HPE inhibits water and ion transport in the cement-based matrix. On the one hand, the low-surface-energy alkyl groups in HPE tend to orient outward on the surfaces of hydration products and pore walls, forming a hydrophobic interfacial layer. This surface arrangement increases the contact angle and weakens the wetting and filling of capillary pores by water. On the other hand, the carboxylate groups in HPE can react with calcium-containing hydration products to generate insoluble precipitated particles in situ. These particles partially fill and block capillary pores, reduce porosity and pore diameter, and change the continuity and

tortuosity of ion transport pathways. Therefore, HPE inhibits water and chloride migration through the combined effects of surface hydrophobization and pore blocking. Under the joint action of increased contact angle, reduced most probable pore size, and lower total porosity, the water-filled connectivity of capillary pores is weakened, thereby reducing water absorption, electrical flux, chloride migration coefficient, and chloride ion concentration in concrete.

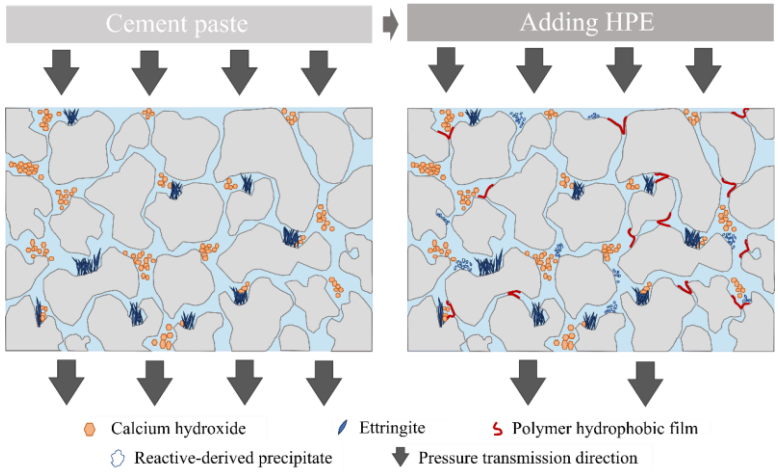

Figure 20. Schematic illustration of HPE inhibiting water and ion transport in the cement matrix

5. Conclusion

This study designed and synthesized a nano-silicon hybrid alkyl carboxylate, denoted as hydrophobic polymer ester (HPE), to improve the resistance of concrete to water ingress and chloride-ion transport. The FT-IR results confirmed the formation of ester carbonyl groups and Si–O–C/Si–O–Si hybrid bonds, indicating the successful construction of an organic–inorganic hybrid structure. The experimental results demonstrated that HPE markedly enhanced the surface hydrophobicity and transport resistance of concrete. With increasing HPE dosage, the contact angle of cement paste increased from 14° to 78° at 1 s and remained at 54° after 30 s, indicating improved resistance to water wetting and absorption. Correspondingly, the long-term water absorption of concrete containing 1.8% HPE decreased to only 28% of that of the reference group. HPE also significantly improved chloride penetration resistance. The electrical flux decreased to 48% of the control value, and the chloride migration coefficient decreased to 62% of the control value. Natural chloride diffusion tests further confirmed that HPE reduced both acid-soluble and free chloride contents within concrete.

Microstructural analyses revealed that the enhanced durability was closely associated with pore refinement, surface hydrophobization, and pore blocking. MIP results showed that the most probable pore diameter decreased from 56.53 nm to 18.17 nm, while total porosity decreased from 22.88% to 16.39%. SEM observations further confirmed the formation of hydrophobic films on pore walls and in-situ precipitated particles within the cement matrix. These effects jointly reduced pore connectivity, weakened capillary suction, and hindered water and chloride transport. Although HPE caused a slight reduction in 28-day compressive strength, the strength loss remained limited compared with conventional hydrophobic admixtures.

6. Declarations

6.1. Author Contributions

Conceptualization, C.R. and Y.M.; methodology, C.R., Y.M., L.Z., R.Y., and Q.P.; formal analysis, C.R., Y.M., L.Z., R.Y., Q.P., and Z.W.; resources, Z.W.; data curation, C.R., Y.M., L.Z., R.Y., and Q.P.; writing—original draft preparation, C.R., Y.M., L.Z., R.Y., and Q.P.; writing—review and editing, C.R., Y.M., and Z.W.; supervision, Z.W. All authors have read and agreed to the published version of the manuscript.

6.2. Data Availability Statement

The data presented in this study are available on request from the corresponding author.

6.3. Funding

This research was financially supported by the National Natural Science Foundation of China: Youth Foundation (52308258).

6.4. Conflicts of Interest

The authors declare no conflict of interest.

7. References

[1] Yi, Y., Zhu, D., Guo, S., Zhang, Z., & Shi, C. (2020). A review on the deterioration and approaches to enhance the durability of concrete in the marine environment. Cement and Concrete Composites, 113. doi:10.1016/j.cemconcomp.2020.103695.

[2] Liu, P., Feng, C., Wang, F., Gao, Y., Yang, J., Zhang, W., & Yang, L. (2018). Hydrophobic and water-resisting behavior of Portland cement incorporated by oleic acid modified fly ash. Materials and Structures/Materiaux et Constructions, 51(2), 38. doi:10.1617/s11527-018-1161-8.

[3] Ruan, S., Gao, R., Tu, W., Li, G., Lu, J. X., Yan, D., & Poon, C. S. (2025). Hydration products and hybridisation mechanisms of hydrophobic cement pastes with alkyl-organosilanes. Cement and Concrete Composites, 163, 106208. doi:10.1016/j.cemconcomp.2025.106208.

[4] Zhao, J., Gao, X., Chen, S., Lin, H., Li, Z., & Lin, X. (2022). Hydrophobic or superhydrophobic modification of cement-based materials: A systematic review. Composites Part B: Engineering, 243, 243. doi:10.1016/j.compositesb.2022.110104.

[5] Cheng, Y., Qin, C., & Huang, Q. (2024). Hydrophobic cement: Concept, preparation and application. Construction and Building Materials, 449. doi:10.1016/j.conbuildmat.2024.138444.

[6] Abdrassilov, D., Aniskin, A., Shakhmov, Z., & Lukpanov, R. (2026). Hydrophobic Modification of Concrete Using a Hydrophobizing Admixture. Construction Materials, 6(1), 3. doi:10.3390/constrmater6010003.

[7] Tittarelli, F., & Moriconi, G. (2011). Comparison between surface and bulk hydrophobic treatment against corrosion of galvanized reinforcing steel in concrete. Cement and Concrete Research, 41(6), 609–614. doi:10.1016/j.cemconres.2011.03.011.

[8] Elnaggar, E. M., Elsokkary, T. M., Shohide, M. A., El-Sabbagh, B. A., & Abdel-Gawwad, H. A. (2019). Surface protection of concrete by new protective coating. Construction and Building Materials, 220, 245–252. doi:10.1016/j.conbuildmat.2019.06.026.

[9] Wang, X., & Lin, Z. (2021). Robust, hydrophobic anti-corrosion coating prepared by PDMS modified epoxy composite with graphite nanoplatelets/nano-silica hybrid nanofillers. Surface and Coatings Technology, 421. doi:10.1016/j.surfcoat.2021.127440.

[10] Wang, D., He, L., Wu, Y., Li, Y., Hu, W., Ma, T., Luo, S., Song, J., Sun, W., & Zhang, G. (2024). Alkali-activated organogeopolymers with volumetric superhydrophobicity. Cement and Concrete Composites, 145, 105336. doi:10.1016/j.cemconcomp.2023.105336.

[11] Zarzuela Sánchez, R., González-Coneo, J., Luna, M., Díaz, A., & Mosquera, M. J. (2023). Studying the bulk hydrophobization of cement mortars by the combination of alkylalkoxysilane admixture and fluoropolymer-functionalized aggregate. Journal of Building Engineering, 65, 105771. doi:10.1016/j.jobe.2022.105771.

[12] Han, K., Yin, B., Jia, X., Xu, H., Li, T., Wang, P., & Hou, D. (2024). One-step hybridization of silane hydrolysis and silica mineralization for enhanced superhydrophobic coating on cement-based materials. Journal of Building Engineering, 94, 109824. doi:10.1016/j.jobe.2024.109824.

[13] Hodul, J., Beníková, T., Drochytka, R., & Borg, R. P. (2025). The Examination of the Effect of Water-Soluble Hydrophobic Agents on Physical–Mechanical Parameters and Resistance to Aggressive Environment of Concrete. Coatings, 15(2), 175. doi:10.3390/coatings15020175.

[14] She, W., Zheng, Z., Zhang, Q., Zuo, W., Yang, J., Zhang, Y., Zheng, L., Hong, J., & Miao, C. (2020). Predesigning matrix-directed super-hydrophobization and hierarchical strengthening of cement foam. Cement and Concrete Research, 131. doi:10.1016/j.cemconres.2020.106029.

[15] Liang, C., Zhao, P., Liu, L., Wang, S., Wang, S., Sobolev, K., & Lu, L. (2023). Fabrication of bulk hydrophobic cement-based materials with ultra-high impermeability. Journal of Building Engineering, 63, 105492. doi:10.1016/j.jobe.2022.105492.

[16] Liang, C., Chen, M., Jiang, D., Hou, P., Zhao, D., Wang, S., Yu, Z., Zhao, P., & Lu, L. (2025). Synthesis of MNS@PDMS emulsion for enhancing hydrophobicity in cementitious materials with limited strength loss. Cement and Concrete Composites, 157, 105875. doi:10.1016/j.cemconcomp.2024.105875.

[17] Zhang, D., Zhu, H., Wu, Q., Yang, T., Yin, Z., & Tian, L. (2023). Investigation of the hydrophobicity and microstructure of fly ash-slag geopolymer modified by polydimethylsiloxane. Construction and Building Materials, 369, 130540. doi:10.1016/j.conbuildmat.2023.130540.

[18] Gao, R., Mao, J., Ruan, S., Tu, W., Wang, Y., & Yan, D. (2025). Early-Age Properties and Reaction of Hydrophobic Portland Cement and Alkali-Activated Fly Ash–Slag Pastes with Alkyl Silanes. Buildings, 15(16), 2966. doi:10.3390/buildings15162966.

[19] Wang, X., Zhang, W., Wang, Y., Wu, H., Danzeng, D., & Meng, Y. (2025). Assessment of the Wettability and Mechanical Properties of Stearic-Acid-Modified Hydrophobic Cementitious Materials. Coatings, 15(1), 100. doi:10.3390/coatings15010100.

[20] Wang, W., Wang, S., Yao, D., Wang, X., Yu, X., & Zhang, Y. (2020). Fabrication of all-dimensional superhydrophobic mortar with enhanced waterproof ability and freeze-thaw resistance. Construction and Building Materials, 238, 238. doi:10.1016/j.conbuildmat.2019.117626.

[21] Meng, F., Han, K., Guo, T., Shu, X., Guo, Y., Dong, L., Cai, J., & Ran, Q. (2025). Elucidating the effects and mechanisms of OTES@silica nano capsules on water resistance and compressive strength of cement paste. Cement and Concrete Research, 198, 108003. doi:10.1016/j.cemconres.2025.108003.

[22] Xie, M., Zhong, Y., Li, Z., Lei, F., & Jiang, Z. (2021). Study on alkylsilane-incorporated cement composites: Hydration mechanism and mechanical properties effects. Cement and Concrete Composites, 122, 104161. doi:10.1016/j.cemconcomp.2021.104161.

[23] Ormellese, M., Lazzari, L., Goidanich, S., Fumagalli, G., & Brenna, A. (2009). A study of organic substances as inhibitors for chloride-induced corrosion in concrete. Corrosion Science, 51(12), 2959–2968. doi:10.1016/j.corsci.2009.08.018.

[24] Diamanti, M. V., Pérez Rosales, E. A., Raffaini, G., Ganazzoli, F., Brenna, A., Pedeferri, M., & Ormellese, M. (2015). Molecular modelling and electrochemical evaluation of organic inhibitors in concrete. Corrosion Science, 100, 231–241. doi:10.1016/j.corsci.2015.07.034.

[25] Bhuvaneshwari, B., Selvaraj, A., Iyer, N. R., & Ravikumar, L. (2015). Electrochemical investigations on the performance of newly synthesized azomethine polyester on rebar corrosion. Materials and Corrosion, 66(4), 387–395. doi:10.1002/maco.201307472.

[26] Zhi, F., Jiang, L., Jin, M., Xu, P., Xiao, B., Jiang, Q., Chen, L., & Gu, Y. (2020). Inhibition effect and mechanism of polyacrylamide for steel corrosion in simulated concrete pore solution. Construction and Building Materials, 259. doi:10.1016/j.conbuildmat.2020.120425.

[27] Chen, R., Liu, J., & Mu, S. (2022). Chloride ion penetration resistance and microstructural modification of concrete with the addition of calcium stearate. Construction and Building Materials, 321, 126188. doi:10.1016/j.conbuildmat.2021.126188.

[28] Chen, J., Zhang, Y., Hou, D., Yu, J., Zhao, T., & Yin, B. (2019). Experiment and molecular dynamics study on the mechanism for hydrophobic impregnation in cement-based materials: A case of octadecane carboxylic acid. Construction and Building Materials, 229. doi:10.1016/j.conbuildmat.2019.116871.

[29] Yang, H.-M., Singh, J. K., Kwon, S.-J., Goudar, S. K., Shivaprasad, K. N., & Lee, S. (2026). Electrochemical and microstructural degradation behaviour of stearate modified cement mortar in chloride environments. Npj Materials Degradation. doi:10.1038/s41529-026-00783-y.

[30] Feng, Z., Wang, F., Xie, T., Ou, J., Xue, M., & Li, W. (2019). Integral hydrophobic concrete without using silane. Construction and Building Materials, 227, 116678. doi:10.1016/j.conbuildmat.2019.116678.

[31] Gong, W., Zhang, Y., Yuan, L., Zhu, B., Yang, H., Hou, Y., Li, H., Lv, Y., & Jin, W. (2025). Study on the preparation and performance of synchronous setting integration in hydrophobic-ordinary concrete. Construction and Building Materials, 504, 144673. doi:10.1016/j.conbuildmat.2025.144673.

[32] Wang, H., Zhang, L., Wang, D., Geng, D., Dong, Z., & Su, Z. (2022). Stability of Phenyl Copolymer-Graphene Oxide Composites in High-Alkali and/or -Calcium Environments: Implications for Strengthening and Toughening Cement-Based Materials. ACS Applied Nano Materials, 5(3), 4038–4047. doi:10.1021/acsanm.2c00023.

[33] Yang, L., Hu, X., Liu, Y., Zhou, D., Yuan, B., Liu, S., Luo, Z., Li, X., Jin, D., & Xu, F. (2026). Multiscale characterization of geopolymers modified with alkali-catalyzed nano-silica: Effects on dispersion and mechanical properties. Cement and Concrete Composites, 165. doi:10.1016/j.cemconcomp.2025.106324.

[34] Hilbig, H., Gutberlet, T., & Beddoe, R. E. (2024). Acid attack on hydrated cement: effect of organic acids on the degradation process. Materials and Structures/Materiaux et Constructions, 57(4), 83. doi:10.1617/s11527-024-02360-8.

[35] Lin, J., Shamsaei, E., Basquiroto de Souza, F., Sagoe-Crentsil, K., & Duan, W. H. (2020). Dispersion of graphene oxide–silica nanohybrids in alkaline environment for improving ordinary Portland cement composites. Cement and Concrete Composites, 106. doi:10.1016/j.cemconcomp.2019.103488.

[36] Mora, E., González, G., Romero, P., & Castellón, E. (2019). Control of water absorption in concrete materials by modification with hybrid hydrophobic silica particles. Construction and Building Materials, 221, 210–218. doi:10.1016/j.conbuildmat.2019.06.086.

[37] Karthick, S., Park, D. J., Lee, Y. S., Saraswathy, V., Lee, H. S., Jang, H. O., & Choi, H. J. (2018). Development of water-repellent cement mortar using silane enriched with nanomaterials. Progress in Organic Coatings, 125, 48–60. doi:10.1016/j.porgcoat.2018.08.021.

[38] Li, H., & Guo, X. (2024). Fabricating hydrophobic silica fume to improve mechanical strength and anti-corrosion of integral hydrophobic cement mortar and its carbon emission assessment. Journal of Cleaner Production, 439, 140857. doi:10.1016/j.jclepro.2024.140857.

[39] Xiang, Y., Duan, H., Yan, C., Zhao, T., & Zhang, H. (2026). Effect of PDMS@PMMA hydrophobic microcapsules on water resistance and hydration characteristics of cement paste. Construction and Building Materials, 506, 145048. doi:10.1016/j.conbuildmat.2025.145048.

[40] Yang, J., She, W., Zuo, W., & Zhang, Q. (2021). Rational application of nano-SiO2 in cement paste incorporated with silane: counterbalancing and synergistic effects. Cement and Concrete Composites, 118, 103959. doi:10.1016/j.cemconcomp.2021.103959.

[41] Zhang, H., Mu, S., Cai, J., & Chen, R. (2021). The impact of carboxylic acid type hydrophobic agent on compressive strength of cementitious materials. Construction and Building Materials, 291, 123315. doi:10.1016/j.conbuildmat.2021.123315.

[42] Zhang, H., Zhou, Y., Mu, S., Cai, J., Hong, J., Liu, J., & Zhao, Y. (2022). Pore Structure and Permeability of Cementitious Materials Containing a Carboxylic Acid Type Hydrophobic Agent. Frontiers in Materials, 9, 907638. doi:10.3389/fmats.2022.907638.

[43] Castro, J., Bentz, D., & Weiss, J. (2011). Effect of sample conditioning on the water absorption of concrete. Cement and Concrete Composites, 33(8), 805–813. doi:10.1016/j.cemconcomp.2011.05.007.

[44] Wang, R., Liu, K., Li, L., He, X., Yang, Y., & Chen, B. (2024). Influence of HPMC on the capillary water absorption, pore structure and hydration of the calcium aluminate cement-hemihydrate gypsum mortar. Journal of Thermal Analysis and Calorimetry, 149(11), 5203–5214. doi:10.1007/s10973-024-13202-8.

[45] Luo, J., Xu, Y., Chu, H., Yang, L., Song, Z., Jin, W., Wang, X., & Xue, Y. (2023). Research on the Performance of Superhydrophobic Cement-Based Materials Based on Composite Hydrophobic Agents. Materials, 16(19), 6592. doi:10.3390/ma16196592.

[46] Yu, Z., Jiang, D., Liang, C., Lu, S., Wu, Y., Wang, K., Zhou, Y., & Zhao, P. (2025). Effects of hydrophobic cement powder on mechanical strength and impermeability of cement-based materials. Construction and Building Materials, 489, 142202. doi:10.1016/j.conbuildmat.2025.142202.

[47] Liu, J., Cai, J., Shi, L., Liu, J., Mu, S., & Hong, J. (2018). The inhibition behavior of a water-soluble silane for reinforcing steel in 3.5% NaCl saturated Ca (OH) 2 solution. Construction and Building Materials, 189, 95-101. doi:10.1016/j.conbuildmat.2018.08.151.

[48] Tittarelli, F., & Moriconi, G. (2010). The effect of silane-based hydrophobic admixture on corrosion of galvanized reinforcing steel in concrete. Corrosion Science, 52(9), 2958–2963. doi:10.1016/j.corsci.2010.05.008.

[49] Zhao, H., Jiang, D., Liang, C., Zhao, D., Yu, Z., Zhang, T., & Zhao, P. (2026). Controllable preparation of engineered hydrophobic slag powder: Synergistically enhancing the strength and impermeability of cement-based materials. Construction and Building Materials, 518, 145825. doi:10.1016/j.conbuildmat.2026.145825.

[50] Yu, J., Li, S., Hou, D., Jin, Z., & Liu, Q. (2019). Hydrophobic silane coating films for the inhibition of water ingress into the nanometer pore of calcium silicate hydrate gels. Physical Chemistry Chemical Physics, 21(35), 19026–19038. doi:10.1039/c9cp03266e.

[51] Yang, C. C., Cho, S. W., & Wang, L. C. (2006). The relationship between pore structure and chloride diffusivity from ponding test in cement-based materials. Materials Chemistry and Physics, 100(2–3), 203–210. doi:10.1016/j.matchemphys.2005.12.032.

[52] Sakai, Y. (2019). Relationship between pore structure and chloride diffusion in cementitious materials. Construction and Building Materials, 229, 116868. doi:10.1016/j.conbuildmat.2019.116868.